

- Requested start date: February 1st, 2024, requested proposal duration: 5 years
- Related Letter of Intent (LOI): None
- Related preliminary proposal: None
- Prime organization: Whittier College
- Primary place of performance:
 - Organization name: Whittier College
 - Country: United States of America
 - Street address: 3406 E. Philadelphia Street
 - City: Whittier
 - State: California
 - ZIP Code: 90602
- Other federal agencies: None
- Other information: Antarctic fieldwork

NSF-CAREER: Translation of Machine Learning and Additive Manufacturing to Accelerate and Diversify Science and Engineering

Radio-frequency (RF) phased-array systems optimized with machine learning have become powerful tools in science and engineering. Recent progress in phased-array radar development has applications in particle astrophysics [1–4], polar research [5, 6], and 5G mobile communications [7]. Phased-arrays are comprised of RF antennas working in tandem to boost received signal sensitivity, and to actively scan transmitted signals without moving parts. There are at least two barriers that impede phased-arrays from enhancing future science and engineering projects on a wide scale. First, the computational electromagnetism (CEM) properties of RF systems are designed with expensive, proprietary software that does not interface with open-source machine learning tools [8]. Second, RF systems are manufactured using costly and time-consuming traditional machining techniques. Ongoing scientific and engineering efforts can be enhanced by a solution that allows machine learning optimization to flourish, reduces design and manufacturing costs, and diversifies participation by reducing financial barriers. Undergraduate education at Whittier College will be enhanced with CEM, machine learning, and 3D printing, as research and educational opportunities will be integrated into the curriculum.

We propose to create the first open-source CEM and additive manufacturing ecosystem capable of 3D-printing phased arrays with conductive filament [8–10]. We have already shown that open-source CEM tools used in photonics can drive the RF phased-array design process [3, 11, 12]. This research will support diverse projects like IceCube Gen2 (radio), Center for Remote Sensing and Systems (CReSIS) missions, and Office of Naval Research (ONR) radar projects. One application in particle astrophysics is the Askaryan Radio Array (ARA), in which phased arrays have increased sensitivity to ultra high-energy neutrino (UHE- ν) interactions in the ice sheet beneath the South Pole [13]. The arrays are vertically polarized, due to mechanical constraints within the ice. Our research could provide a *horizontally polarized* design that overcomes the mechanical constraints through machine learning, boosting the chances of making the first UHE- ν observations in history [14]. This research will *accelerate and diversify* research in UHE- ν , climate science, and RF engineering by *translating* successes in CEM and materials research. This work will be integrated into our curriculum and research programming at Whittier College, a Title-V Hispanic Serving Institution (HSI).

This work will provide research and educational opportunities to diverse undergraduates at Whittier College. We have a proud tradition of providing access to higher education to Spanish-speaking and historically marginalized students, and we are the only HSI member of the IceCube Gen2 collaboration. People of color and first-generation students make up 63% and 29% of our student body, respectively. Internal assessment studies indicate that students of color receive lower grades than their peers in introductory STEM courses. We have learned from workshops hosted by the Cottrell Scholars Network that emphasizing the dignity and self-efficacy of diverse students can increase their performance [15, 16]. Emphasis in these areas makes students feel they *belong* in our courses, despite encountering adversity. In keeping with the theme of *translation*, and in order to emphasize the dignity of our students no matter their background, we seek to create a bilingual (Spanish and English) mobile application (app) that introduces STEM concepts within a welcoming digital environment.

There is precedent for learning apps enhanced by machine learning in the Duolingo method for language and mathematics [17]. We seek to provide data insights about student learning to instructors through the app, which will lead to more efficient and customized classroom instruction. A prototype application is being built by Whittier College undergraduates. The creation and implementation of this program represents an opportunity for Whittier College students to enhance the learning experience for their peers while gaining valuable coding and machine learning experience. In addition to algorithms presented within the Duolingo method, the educational data mining (EDM) literature provides examples of apps that boost engagement and success in introductory STEM courses [18–21]. Members of our community have shared that translating mathematics and physics exercises into Spanish aids in solving them. Our application will boost their skills and build confidence by offering them engaging, game-like physics training in the language of their choice. Finally, we propose to create a bilingual lecture series and recruitment events designed to welcome the broader community into the Whittier College environment.

Translation of Machine Learning and Additive Manufacturing to Accelerate and Diversify Science and Engineering

Jordan C Hanson, PhD
Assistant Professor of Physics and Astronomy
Whittier College
Whittier, CA

June 1, 2023

Contents

1 Project Description: Intellectual Merits	3
1.1 Computational Electromagnetism and Additive Manufacturing	4
1.1.1 RF Laboratory Capability and Prior ONR Funding	7
1.2 The Connection to Ultra-high Energy Neutrino Observations	8
1.3 The Connection to Remote Sensing of Ice Sheets	10
1.4 Integration of Research and Education at Whittier College	12
1.5 Timeline and Project Planning, Intellectual Merits	12
2 Project Description: Broader Impacts	13
2.1 Translation of Scientific and Engineering Research	13
2.2 Mobile Application Development	13
2.3 Bilingual Public Lectures and Recruitment Events	13

Project Description: Intellectual Merits

Radio-frequency (RF) phased arrays have applications in radar telemetry, telecommunications, ground-penetrating radar, scientific instrumentation, and remote sensing [1, 2, 5, 13, 22–24]. In the one-dimensional case, N three-dimensional RF antennas are arranged in a line with fixed spacing. In the two-dimensional case, $N \times M$ three-dimensional antenna elements are arranged in a two-dimensional grid with fixed spacing in both dimensions. The signal to noise ratio (SNR) of received signals in arrays of dimension N is boosted by a factor of $\approx \sqrt{N}$, because the N signals are combined coherently while thermal noise adds like \sqrt{N} . The SNR boost is critical for certain kinds of scientific observations. For example, systems created at the Center for Remote Sensing and Integrated Systems (CReSIS) are flown in polar regions to perform radar sounding of ice sheets for the purposes of geophysics and climate science [5]. Reflected signals carry information about the ice depth, temperature, and internal structure of the ice. The radio echoes have small SNR values that require phased arrays.

Traditionally, RF phased arrays are designed with commercial computational electromagnetism (CEM) software. Radio antennas and phased arrays have *radiation patterns* that define directions of maximum transmission power and received sensitivity. Radiation patterns have a main lobe in which most of the radiation is concentrated, and the angular width of the main lobe is called the beam width. Other parameters like S-parameters quantify the efficiency of the systems. CEM packages like XFDTD and HFSS are used to model these properties as a function of frequency [25, 26]. The XFDTD package, for example, relies on the finite difference time domain (FDTD) method. The FDTD approach is a CEM technique in which spacetime and Maxwell's equations are broken into discrete form. HFSS uses a similar approach in the Fourier domain, the Finite Element Method (FEM). Depending on the software license and version, the current price of these products ranges between \$5,000 and \$40,000 USD. These costs are prohibitive for HSI undergraduate institutions like Whittier College. Removing this financial barrier to entry would enable diverse researchers to gain important skills in the field of RF design.

Another drawback of commercial CEM software is the lack of access to the source code, which impedes the incorporation of modern machine learning packages. Phased array properties are determined by the shape of the RF elements and the grid properties of the array, and the parameter space is driven by the complex variety of RF element shapes. When combined with open-source CEM software, modern machine learning algorithms can locate optimal solutions within the parameter space. The authors of [8] review a number of open-source CEM packages, and conclude that there are viable open-source options for simple RF antenna shapes. For our proposed work, the open-source CEM software must be able to handle the growing complexity of RF antenna designs. One interesting choice is the MIT Electromagnetic Equation Propagation (MEEP) package [12]. Though MEEP was designed for μm wavelengths in photonics applications, we have shown that the scale-invariance of Maxwell's equations allows MEEP users to translate designs to wavelengths at the cm-scale. We have also shown that MEEP can drive the RF phased-array design loop, and that 3D printer schematics can be extracted from this process [3, 11, 12]. This research represents an opportunity for diverse undergraduates to gain experience applying machine learning tools to the design of practical systems.

Recent advances in materials research have led to the creation of 3D printer filament that has conductivity in RF bands. Funded through an NSF Translational Impact (TI) award (1721644), Multi3D LLC. has

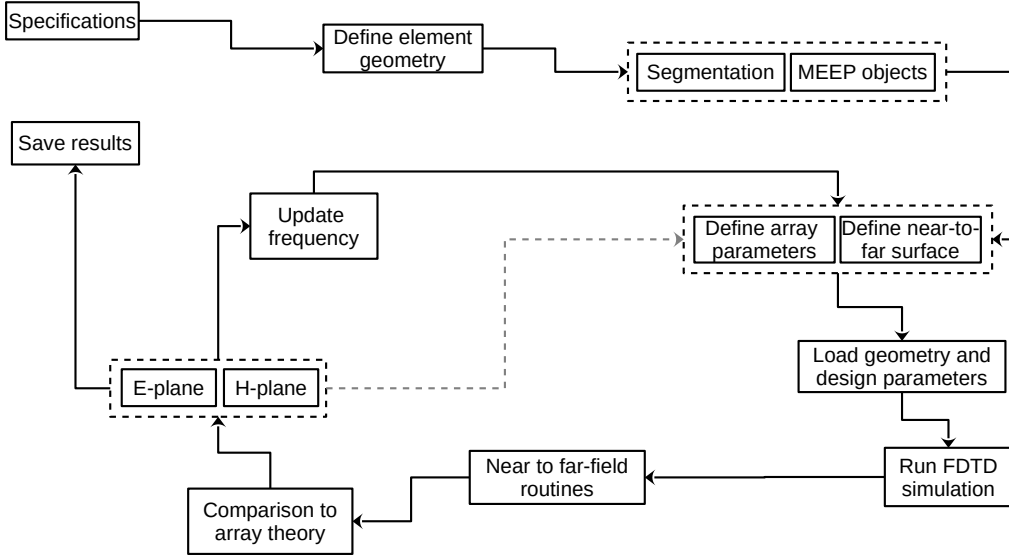


Figure 1.1: Our design process for RF phased arrays from [3], adapted from Fig. 1 of the review [8].

produced filament with a resistivity of just $10^{-2}\Omega\text{ cm}$: the Electrifi filament. Several antenna designs have already been produced [10, 27]. These examples include horn antennas with gain factors of 15 dB at 5.8 GHz, and microstrip patch antennas with gains of 1-2 dB at 2.5 GHz. The results match expectations from HFSS models, exhibiting no major differences with antennas made using perfect conductors. There are, however, virtually no examples of 3D printed RF phased arrays in the [0.1 - 1] GHz bandwidth. This bandwidth is the most relevant for the aforementioned applications in particle astrophysics and geophysics. Further, whole new designs can be discovered that improve on designs like the horn and patch antennas by merging machine learning packages with MEEP. In Sec. 1.1, we review progress already made at Whittier College. In Sec. 1.2, we show how this work enhances the field of UHE- ν observations. In Sec. 1.3, we show how this work enhances the field of radio echo sounding of ice sheets and ice shelves. In Sec. 1.4, we articulate our vision for the integration of this research into our STEM curriculum at Whittier College. In Sec. 1.5, we provide a general project timeline, broken into manageable phases. In Sec. 1.5, we make the case that the merits of our proposed project phases are sound, and useful to multiple fields.

1.1 Computational Electromagnetism and Additive Manufacturing

In Summer 2020, we received a Faculty Fellowship from the Office of Naval Research (ONR) to study and design phased arrays in the [0.1 - 5] GHz bandwidth. This bandwidth is relevant for projects like IceCube Gen2 (radio), and Whittier College is a member institution of the IceCube Gen2 collaboration. With our background in NSF-funded projects like the Antarctic Ross Ice Shelf Antenna Neutrino Array (ARIANNA), the Askaryan Radio Array (ARA), and NASA-funded projects like the Antarctic Impulsive Transient Antenna (ANITA), we were qualified to teach our ONR colleagues about phased array applications. Our goal was to design a phased array system to be integrated as a transmitter in an anechoic chamber. The anechoic chamber will serve as a testing facility for active radar systems. We began by giving lectures on the electromagnetism of phased arrays and scientific and engineering applications. The audience included engineers and programmers that work in acquisition and development for the Naval Surface Warfare Center (NSWC), Corona Division (NSWC Corona). Our design flow is depicted in Fig. 1.1. To minimize costs and increase access to Whittier College students, we decided to investigate open-source CEM options for the design.

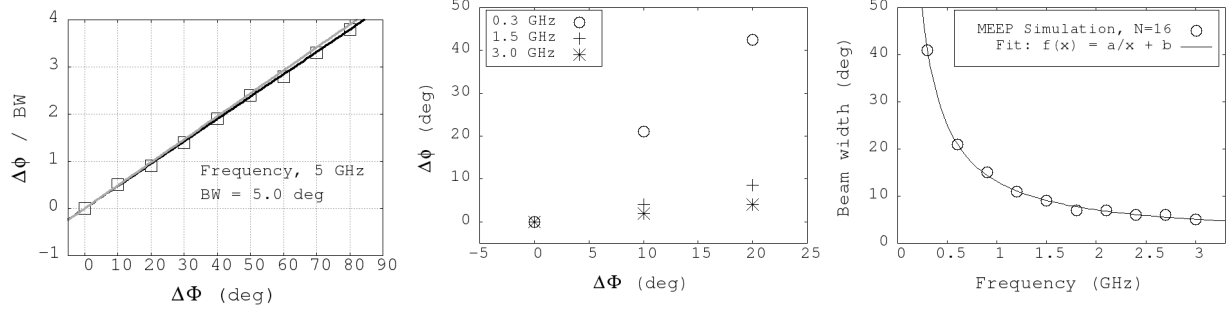


Figure 1.2: (Left) The beam angle $\Delta\phi$ divided by the beam width BW for the $N = 16$ one-dimensional Yagi array versus $\Delta\Phi$, the phase shift per element. The gray line represents theoretical expectation, and the black line is a linear fit to the data. (Middle) $\Delta\phi$ versus $\Delta\Phi$ for the $N = 16$ version of the one-dimensional horn array, for several frequencies. (Right) The dependence of the beam width on frequency for the one-dimensional $N = 16$ horn array. The black line is a functional fit to the data $f(x) = a/x+b$ with $a = 12.0 \pm 0.1$ degree GHz, and $b = 1.1 \pm 0.2$ degrees.

We encountered the aforementioned review article in the open-access journal *Electronics* that indicated there are open-source CEM tools that can be adapted to phased array analysis. Our design flow in Fig. 1.1 is adapted from Fig. 1 of the review to include specific tasks required for phased arrays, and algorithms for the computation of far-field radiation patterns. MEEP was noted by the authors in the review as the most advanced among open-source FDTD programs, but they did not benchmark it against HFSS or XFDTD due to the “steep” learning curve. As part of the ONR Summer Faculty Fellowship, we ascended the learning curve and adapted MEEP to RF systems. The key insight was that MEEP takes advantage of the *scale invariance* of Maxwell’s Equations. The simplest way to understand this is to understand how MEEP uses relative units when discretizing Maxwell’s equations for Python code.

Like other FDTD CEM methods, MEEP uses a Yee lattice to discretize Maxwell’s equations [28]. When the speed of light is set to unity ($c = 1$), distance and time units are set to be the same. Frequency and wavelength units are the inverse of each other. But distance and wavelength can take *any* unit of length in the Yee lattice. Most MEEP users interpret this unit of length to be $1 \mu\text{m}$ because the applications are for photonics. For example, a *relative* frequency (unit-less) of 0.5 corresponds to a *relative* wavelength of 2. When interpreted as $2 \mu\text{m}$, the frequency is 150 THz in real units that correspond to optical bandwidth. If we choose to interpret the *relative* wavelength as 2 cm, the real frequency is 15 GHz. A *relative* frequency of 0.05 corresponds to the RF frequency 1.5 GHz. Assuming design components have sufficient conductivity at RF frequencies, we have re-purposed MEEP as an RF simulator.

By Fall 2020, we were producing CEM models using MEEP that matched expected phased array properties. For a one-dimensional array with N elements, there is a linear relationship between the radiated plane-wave direction $\Delta\phi$, and the phase shift per element $\Delta\Phi$. The coefficient of the relationship is determined by the ratio of real wavelength to element spacing. Figure 1.2 contains results for our first phased array models in which the elements were Yagi-Uda style antennas and horn antennas. The linear relationship is evident in the data. The radiated signal direction $\Delta\phi$ is divided by the beam width (BW) in Fig. 1.2 (left), and is left in degrees in Fig. 1.2 (middle). A beam width of a radiation pattern is the angular width of the main lobe, outside of which the radiated power has decreased by 3 dB. In Fig. 1.2 (left), the $N = 16$ Yagi array can steer a 5 GHz plane wave up to four beam widths to the right or left of the forward direction. Yagi-Uda style antennas are designed for a single frequency. In Fig. 1.2 (middle), results are shown for an $N = 16$ array of horn antennas. Since horn antennas are broadband radiators, the linear relationship is shown for 0.3, 1.5, and 3.0 GHz. The beam width is inversely related to frequency, so $\Delta\phi$ was left in degrees. In Fig. 1.2 (right), the inverse relationship is shown.

We can also produce phased array radiation patterns with MEEP that match theoretical expectations. The radiation pattern of a one-dimensional array of N radiating point sources can be derived using first principles [3]. The *pattern multiplication theorem* states that the radiation pattern of a one-dimensional

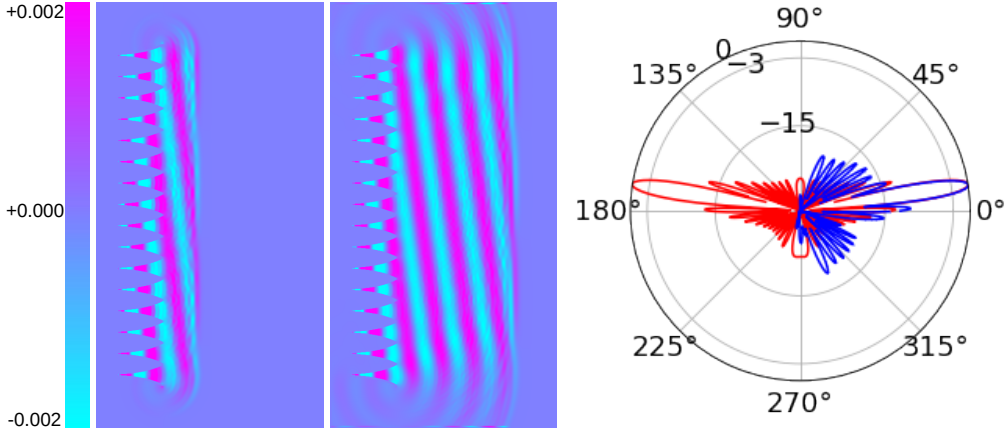


Figure 1.3: (Left) The $N = 16$ one-dimensional horn array, radiating a linearly polarized electric field $\vec{E}(x, y, t)$ (y-component shown, in arbitrary units) at $t = 1$ ns into the simulation run, and (middle) at $t = 2$ ns into the run. The 2D area is $80 \times 150 \text{ cm}^2$. The frequency is 2.5 GHz, and the beam angle is $\Delta\phi = 9$ degrees from broadside (x-direction). (Right) The normalized radiated power in dB versus $\Delta\phi$. The blue curve represents the results from MEEP, and the red curve is the theoretical expectation from N point sources.

phased array of N identical elements will be that of a row of N point sources, multiplied by the radiation pattern of the individual element. In Fig. 1.3 (left and middle), the radiated field of a $N = 16$ horn array is shown in the E-plane (x-y plane). The radiation pattern is shown in 1.3 (right). The main lobe is steered 9 degrees above the x-axis, matching the theoretical expectation. The blue curve in the polar plot represents the CEM radiation pattern from MEEP, while the red curve is the theoretical expectation from a row of N point sources. The row of point sources is symmetric, creating a back lobe at $\Delta\phi = 171$ degrees. The horn array has no back lobe because the individual horns suppress backward radiation, as expected from the pattern multiplication theorem. We also showed that two-dimensional arrays of Yagi-Uda and horn antennas matched theoretical expectations exactly. Our revelation that the photonics code MEEP could be used to design phased arrays design earned the final article Top 10 honors for December 2020 to May 2021 from the editors of *Electronics*.

In Summer 2021, we again received a Faculty Fellowship from the ONR to continue this work. We focused on creating realistic 3D models of horn antennas that could be printed with 3D printers. Working with undergraduate researchers, we learned to create designs that can be expressed as Python3 functions and converted to a GDSII CAD file. GDSII files can be imported into MEEP, and converted to STL files for use with a 3D printer. Our CEM codes are therefore using the precise shape that we intend to print. We acquired NinjaTek proto-pasta 3D printer filament, advertised as conductive. We printed a horn with in-built SMA connector for RF cables (Fig. 1.4). The proto-pasta result had the right shape, but a measured resistance too large for an RF antenna. Multi3D LLC, the manufacturer of the Electrifi filament, has now provided resistivity results that compare proto-pasta with Electrifi (Fig. 1.5). The Electrifi filament will improve resistivity by two orders of magnitude. We seek to print Electrifi-based antennas, and to measure the radiation pattern and S-parameters.

In Summer 2022, we received a final ONR Faculty Fellowship that focused on GPS M-code and modernization. Alongside this work, we continued to refine the open-source RF horns. This included computing radiation patterns and S-parameters for the full 3D horns stored in CAD files. In Fig. 1.6 (a), the main lobes are designed to point to 0 degrees (x-direction) for the E-plane (x-y plane), and 90 degrees for the H-plane (x-z plane). The E-plane is the plane containing the linearly polarized radiation vector, and the H-plane is orthogonal to the E-plane. In Fig. 1.6, the (voltage standing wave ratio) VSWR is shown. The VSWR is a common figure of merit for RF antennas, related to the S11 scattering parameter. The VSWR approaches 1 for an efficiently radiating antenna. The radiation patterns match expectations for horn antennas (see Fig. 19 of [10]). The VSWR results demonstrate efficient radiation in the bandwidth [0.5 - 6]

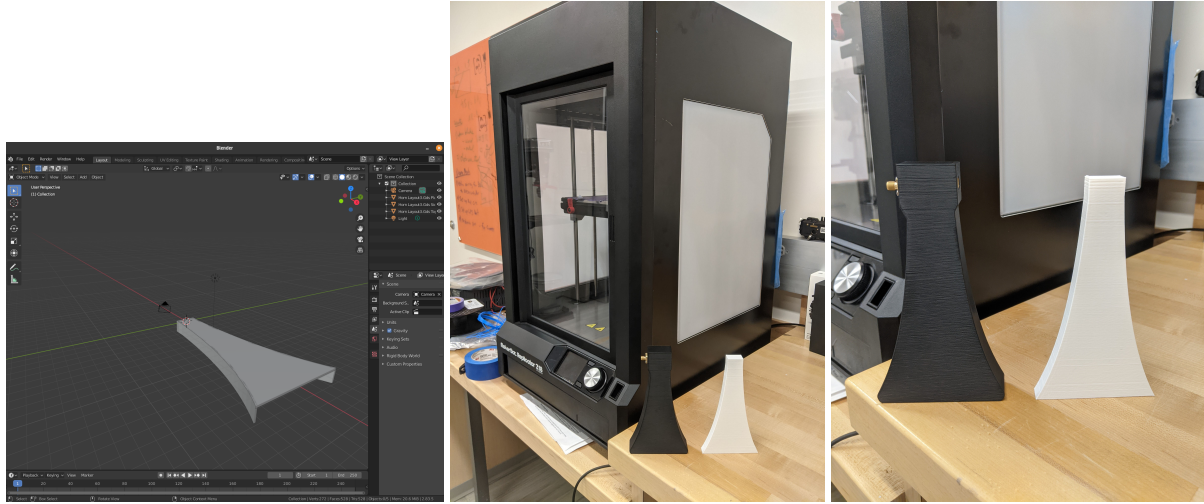


Figure 1.4: (Left) Blender/STL files extracted from MEEP code. (Middle) MakerBot 3D printer, with PLA horn model (white), and proto-pasta with SMA connector (black). (Right) Close-up of horns.

GHz. We presented our progress at the annual MeepCon 2022 at the Massachusetts Institute of Technology (MIT) [11]. We learned the extent to which MEEP can be integrated with Python3-based machine learning tools [29], and how eager MEEP developers are to collaborate in the RF regime. Extending MEEP to RF users widens the user base of MEEP, which has traditionally focused on photonics applications.

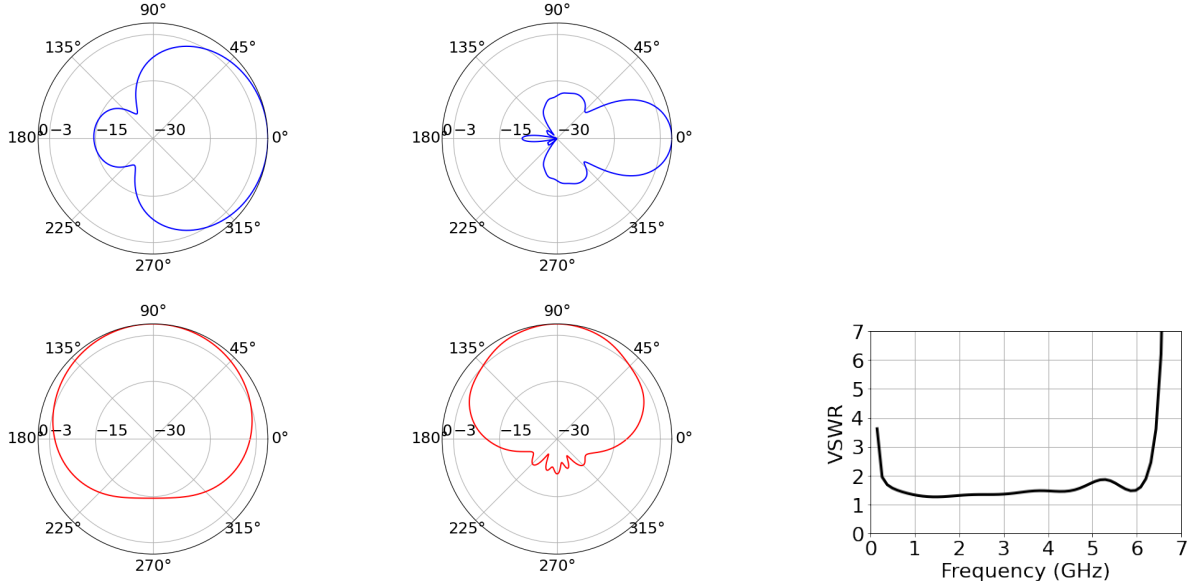
1.1.1 RF Laboratory Capability and Prior ONR Funding

As of May 2023, we have officially begun an Educational Partnership Agreement (EPA) between NSWC Corona and Whittier College. As part of the EPA, NSWC Corona has the ability to transfer laboratory equipment to Whittier College. NSWC Corona has provided RF bench testing equipment that is perfectly suited to the proposed work (see Tab. 1.1). Our network analyzer and power sensors can perform S-parameter measurements over a bandwidth that encompasses the proposed bandwidth of [0.1 - 5 GHz] for our antennas under test (AUT). Our signal generator can create calibration signals for our calibration antennas and AUT in the proposed bandwidth. Our systems come with calibration antennas that serve as benchmark devices for comparison to the AUT we create via 3D printing. Due to the precision and wide bandwidth of these devices, they require calibration. Our calibration kits serve this purpose. Our laboratory is therefore already outfitted for the RF testing and calibration required to complete the proposed projects. This minimizes the impact of new equipment in our proposed budget.

Horizontal Traces	Dimension ($X \times Y \times Z$ cm 3)	Resistance (Ω)	Resistivity (Ω cm)
Electrifi	0.2 × 10 × 0.2	3.0	0.012
Black Magic 3D	0.2 × 10 × 0.2	142.5	0.57
Proto-Pasta	0.2 × 10 × 0.2	1506	6.02

Vertical Towers	Dimension ($X \times Y \times Z$ cm 3)	Resistance (Ω)	Resistivity (Ω cm)
Electrifi	0.5 × 0.5 × 10	3.4	0.085
Black Magic 3D	0.5 × 0.5 × 10	103.6	2.59
Proto-Pasta	0.5 × 0.5 × 10	410	10.25

Figure 1.5: Resistivity results published by Multi3D LLC that compare the proto-pasta product with the new Electrifi conductive filament (<https://www.multi3dffc.com/faqs/>).



(a) Radiation pattern results using GDSII/CAD for (top left) E-plane at 0.5 GHz, (top right) E-plane at 5.0 GHz, (bottom left) H-plane at 0.5 GHz, (bottom right) H-plane at 5.0 GHz. See text for details.

(b) The VSWR figure of merit versus frequency in GHz for the RF horn.

Figure 1.6: Results for RF horn design, using the open-source design process open to 3D printing.

Equipment	Bandwidth	Cost
Rohde and Schwartz ZVL6 Network Analyzer	9 kHz to 6 GHz	\$20k
Rohde and Schwartz NRP-91 Power Sensors (2)	9 kHz to 6 GHz	\$8k
Aeroflex 3416 Digital RF Signal Generator	250kHz to 6 GHz	\$12k
Calibration antenna kits (2)	Varies by antenna	\$2k
Calibration test kits for Network Analyzer (2)	6 kHz to 9 GHz	\$6k

Table 1.1: A listing of the equipment provided to our labs by the Office of Naval Research.

According to ONR policy, Faculty Fellows who have received fellowships three years in a row must take a mandatory gap year. In Summer 2024, we will be eligible for Senior Faculty Fellowships because we received regular Faculty Fellowships in the Summers 2020-22. Our EPA contacts with NSWC Corona have indicated that our focus will broaden to include cybersecurity and reliability engineering projects. These projects will be in the form of student internships, curricular enhancements, and summer research projects. Given the connections to particle astrophysics and geophysics, it is wise to organize the proposed work under the NSF CAREER program, so that it will maintain this focus. We provide a summary of funding received related to this project in Tab. 1.2. Note the regular involvement of undergraduate researchers. These researchers have diverse majors and interests, including our 3-2 Engineering Program (Wildanger), Physics and Math double major (Hartig), and Math/Integrated Computer Science (Gómez-Reed) and Householder), and Physics and Astronomy (Goodman and Smith).

1.2 The Connection to Ultra-high Energy Neutrino Observations

The flux of neutrinos with energies between [0.01-1] PeV has been detected by IceCube [30]. The UHE- ν flux could potentially explain the origin of UHE cosmic rays (UHECR), and represents an opportunity to study electroweak interactions at record-breaking energies [31,32]. Previous analyses have shown that the discovery of UHE- ν above 1 PeV will require an expansion in detector volume, because the UHE- ν flux is

Student/Professor	Grant Opportunity	Amount	Dates
Jordan C. Hanson	ONR Summer Faculty Fellow	\$16.5k	Summer 2022
Dane Goodman	Summer researcher	Course credit	Summer 2022
Andrew Householder	Summer researcher	Course credit	Summer 2022
Raymond Hartig	Ondrasik-Groce Fellowship	\$5k	Summer 2022
Jordan C. Hanson	ONR Summer Faculty Fellow	\$16.5k	Summer 2021
Adam Wildanger	Fletcher Jones Fellowship	\$5k	Summer 2021
Jordan C. Hanson	ONR Summer Faculty Fellow	\$16.5k	Summer 2020
Raymond Hartig	Fletcher Jones Fellowship	\$5k	Summer 2020
John Paul Gómez-Reed	Ondrasik-Groce Fellowship	\$7.5k	Summer-Fall 2019
John Paul Gómez-Reed	Keck Fellowship	\$5k	Summer 2018
Cassady Smith	Keck Fellowship	\$5k	Summer 2018

Table 1.2: A listing of the grant opportunities awarded to our group for RF design, software development, and machine-learning. All students are at the undergraduate level.

expected to decrease with energy [33–37]. Whereas the current version of IceCube detector observes neutrinos via optical signals that travel < 100 m, the Askaryan effect translates a UHE- ν interaction into an RF pulse that travels more than 1 km in RF-transparent media such as Antarctic and Greenlandic ice [38–40]. Utilizing the Askaryan effect therefore allows for detectors with vastly larger effective volumes than optical observations.

The Askaryan effect occurs when a neutrino with velocity larger than the speed of light in a dielectric medium initiates a high-energy cascade with negative total charge. The charge radiates energy in the RF bandwidth [41, 42]. The IceCube EHE analysis has constrained the UHE- ν flux to be $E_\nu^2 \phi_\nu \leq 2 \times 10^{-8}$ GeV cm $^{-2}$ s $^{-1}$ sr $^{-1}$ between $[5 \times 10^{15} - 2 \times 10^{19}]$ eV [35]. Arrays of $\mathcal{O}(100)$ *in situ* detectors encompassing effective areas of $\approx 10^4$ m 2 sr per station, spaced by $\mathcal{O}(1)$ RF attenuation length could discover a UHE- ν flux beyond the EHE limits. Polar ice formations in Antarctica and Greenland have the longest attenuation lengths. A group of prototype Askaryan-class detectors has been deployed in polar regions that seek to probe unexplored UHE- ν flux parameter-space [36, 37, 43, 44].

Askaryan radiation was first observed in laboratory settings [45–47]. The RF pulse shape is influenced by the shape of the cascade, and the observed pulse is strongest when viewed close to the Cherenkov angle. Working with an undergraduate researcher, we recently published a theoretical model of the electromagnetic field of Askaryan radiation [48]. Askaryan models are incorporated into simulations like AraSim in order to calculate expected signals and aid in detector design [49–51]. For example, software developed for IceCube Gen2 (radio) utilizes machine learning and the Askaryan pulse shape to provide a way to reconstruct UHE- ν properties in future data [14, 52, 53]. Askaryan electromagnetic fields are combined with RF channel responses to form “signal templates” used to search large data sets for signal candidates [36, 54]. Data sets are large for Askaryan-class detectors due to the inevitable RF thermal background data. For Askaryan signals, the SNRs at RF channels are expected to be small (SNR ≈ 3), because the amplitude of the Askaryan field decreases with the distance to the UHE- ν interaction, and the signal is attenuated by the ice [38, 55, 56]. Template-waveform matching between models and data is a powerful technique for isolating high-energy particles [54, 57, 58].

Phased arrays have been incorporated into Askaryan-class prototype detectors, after it was noted that phased arrays would enhance the probability of observing UHE- ν [1, 2]. Phased arrays boost the SNR of observed signals by combining multiple observations of the same RF pulse coherently. Examples of this strategy are ARA5 [13], and the first deployments of Radio Neutrino Observatory, Greenland (RNO-G) [59]. The arrays in each are identical, vertically polarized dipole antennas. These decisions were made for mechanical reasons, because the array must fit in a 100 m deep, vertically-drilled borehole in the ice. The radiation pattern exhibits azimuthal symmetry, and there is no sensitivity to the horizontal Askaryan field component. Further, the designs assume a uniform index of refraction for the ice surrounding the array. As part of our proposed work, we seek to use machine learning to discover horizontally polarized array designs that fit into the borehole and account for the index of refraction, n .

We included a short study of phased array behavior in the South Pole ice environment in our recent publications [3, 11, 12]. Most commercial CEM packages assume a uniform n in the surrounding medium. By contrast, MEEP gives the user 3D control of the index of refraction, $n(x, y, z)$. The RF index of refraction varies with the depth (z) near the snow surface. The $n(z)$ function is well-measured in a variety of locations in Antarctica [60], and Greenland [61]. ARA (South Pole) [13], RNO-G (Greenland) [59], and IceCube Gen2 (radio) (South Pole) [62] can all benefit from designs that account for $n(z)$ and have sensitivity to the horizontal component of the Askaryan field.

The common simulation package used for ARA, RNO-G, and IceCube Gen2 is NuRadioMC, built from prior experience with ARA and ARIANNA [37, 40, 51, 63, 64]. NuRadioMC addresses analytically the ray-tracing solution for UHE- ν signals as they propagate through polar ice. We derived the analytic ray-tracing solutions presented in [51] and [60], which were adopted into NuRadioMC. A goal of our proposed research will be to incorporate realistic, 3D field propagation into NuRadioMC using FDTD computations with MEEP, with our analytic Askaryan model as the MEEP source [48, 65]. This integration should boost the accuracy of the computations made with NuRadioMC, which will be matched with future ARA, RNO-G, and IceCube Gen2 data to isolate UHE- ν signals.

1.3 The Connection to Remote Sensing of Ice Sheets

A gap exists in Askaryan-based UHE- ν science. A knowledge of the RF attenuation length, λ , versus frequency, depth, and location is paramount to understanding UHE- ν detector sensitivity. Although we have made detailed measurements of λ versus frequency [38, 39, 66], we do not scan detector volumes to measure this parameter versus geographic location: $\lambda(x, y)$. Further, $\lambda(z)$ is merely inferred from the average attenuation and ice core temperature data (see Fig. 24 from [40]). IceCube Gen2 (radio) will require $\lambda(x, y, z)$ to be measured precisely. CReSIS radio sounding data, available on the Open Polar Server (OPS: <https://ops.cresis.ku.edu/>), have been used to constrain $\lambda(x, y)$ across Greenland [67]. Far less CReSIS data is available near the location of IceCube (South Pole), due to the complex logistics of organizing flights in that region. A new technological effort to incorporate radio sounding instrumentation into unmanned aerial systems (UAS) is underway, and it can benefit geophysics and particle astrophysics.

UAS systems offer a way to enrich radio sounding data for geophysics and particle astrophysics. OPS radio sounding data is generated from human-piloted fixed-wing aircraft with straight flight lines that carry on-board radar. Flight lines can be hundreds of kilometers long, scanning wide areas with synthetic aperture radar (SAR) techniques. There are, however, three key disadvantages. First, there may not be a flight near the desired location, which is the case for South Pole. Second, flights only give a snapshot of the ice at the time, and aircraft may not return to the same location for several years. Third, the bandwidth of the radar does not always overlap with the bandwidth desired for IceCube Gen2 (radio). Dedicated UAS could constrain $\lambda(x, y)$ in both the temporal and spatial regimes. UAS are able to hover and fly at lower altitudes, so they can collect a wider variety of data than traditional fixed-wing craft. For example, the CReSIS ultra-wide band (UWB) Snow Mini radar system was integrated onto the AeroVironment Vapor 55 UAS. The low altitude flight capability increases the SNR in difficult areas by pushing clutter angles outside the field of view. The SNR is also boosted by hovering due to increased integration time over a single site [5]. The average cost of the Vapor 55, however, is about \$90k USD.

In our RF design lab at Whittier College, our group has already constructed a 3D printed drone using PLA, carbon-fiber tubing, commercial motors, and commercial transmitters. The unit has ≈ 1 kg payload, a 20-min flight time, and is powered by LiPo batteries, for a total cost of ≈ 1 k USD (see Fig. 1.7). Before the onset of the COVID-19 pandemic paused in-person laboratory work, we had plans to equip it with solar charging and cold-temperature components. Thus, there is a potential for collaboration between CReSIS and IceCube Gen2 (radio) to solve a common problem: the solar rechargeable $\lambda(x, y)$ measurement system with vertical take-off and landing (VTOL). Our drone design can be 3D printed and assembled from commercial parts for ≈ 1 k with VTOL, but we need valuable insights from the CReSIS group on retro-fitting for cold temperatures and solar charging. When outfitted with a 3D-printed phased array radar, we will have a formidable system capable of filling gaps in our knowledge of polar ice sheets.



Figure 1.7: Our 3D-printed quad-rotor drone, designed and assembled by Whittier College undergraduates using our RF design lab and machine shop. The unit is equipped with hand-held RC control, and GPS with programmable waypoints.

Phased array radio sounding systems mounted on UAS will be highly useful for polar research, but these designs face engineering limitations that must be overcome. The optimization of craft weight, thrust, payload, and flight time is the primary problem to be solved. To collect quality radio sounding data, the payload must be flown horizontally for 1 – 10 km, implying ≈ 1 hr battery life at reasonable speeds. The requirement for longer flight times drives up battery size. Increased battery size increases weight, which tends to decrease flight time. Phased array payloads with a large number of elements could benefit data collection, but increased payload adds weight and decreases flight time. The optimization is made far easier if the radar transmitter and receiver system is integrated into the hull of the UAS. We propose to study how the RF phased array can be printed into the hull of the UAS, using machine learning to optimize beam-forming for radio sounding. The Electrifi filament has a similar density to aluminum, meaning it can serve as *both* a structural component, and phased array. Manufacturing structural components as phased array elements reduces costs and weight. This idea would reduce payload, thereby facilitating the effort to minimize radar units for UAS integration.

As part of this engineering effort, we also propose to simulate expected results using MEEP. Performing a CEM simulation that incorporates our current knowledge of ice properties with the radar response would enrich the research in two ways. First, such simulations enhance the design process, revealing design requirements, shortcomings, and ways to overcome them. MEEP simulations require the user to specify the complex matrix for the dielectric constant of the medium, $\epsilon(x, y, z)$. The ϵ matrix determines how RF waves reflect, refract, and propagate back to the receiver. Optimizing UAS phased array design for maximal $\epsilon(x, y, z)$ precision will result in optimal precision for $\lambda(x, y, z)$. For dielectric materials, ϵ and λ are related analytically [38]. Second, matching MEEP simulation output to data collected in the field will provide a cross-check between the observed $\epsilon(x, y, z)$ and the simulated $\epsilon(x, y, z)$.

FDTD simulations are notorious for consuming computational resources like volatile memory, while providing the necessary resolution for $\epsilon(x, y, z)$, and electromagnetic fields versus time, frequency, and space. At Whittier College, we have acquired a System76 Helio with AMD Ryzen threadripper 3990x 64-core, 128 thread processor. The system has 0.5 GB of volatile memory per thread. We have already shown that running MEEP in parallel on our system reduces run times by an order of magnitude [11]. The reduction is due primarily to increased set up speed for $\epsilon(x, y, z)$. Thus, we are already in a position to perform such CEM simulations quickly and efficiently.

1.4 Integration of Research and Education at Whittier College

It is important to note that our undergraduate physics, computer science, and engineering curriculum is greatly enhanced by researching applications of CEM. One straightforward example is to incorporate CEM tools like MEEP into lower and upper division electromagnetism and Python3 courses. Our 3-2 Engineering Program students, Physics majors, and Integrated Computer Science (ICS) majors all stand to benefit from learning to use Python to perform computational physics. Our current curriculum does not yet include CEM in lower or upper-division electromagnetism courses, nor is it included in computational physics. Integrating results from this research into course management systems, via MEEP Jupyter notebooks, is a straightforward way to enhance STEM education for our diverse undergraduates. Showcasing the 3D printed RF systems should engage their curiosity by providing a real-world application of course concepts. Finally, given the diverse demographics of our students, enriching their educational experience with real-world applications serves to diversify the STEM workforce. We propose to develop project-based learning (PBL) modules that incorporate RF design, machine-learning, and additive manufacturing for our Whittier College STEM students.

1.5 Timeline and Project Planning, Intellectual Merits

Example

Project Description: Broader Impacts

Overaching Introduction

2.1 Translation of Scientific and Engineering Research

Do people really know how multi-lingual this area is, and why that is important? Cite the creation of *History of Science in Latin America*.

2.2 Mobile Application Development

Educational Application for Systematic Training and Learning of STEM (EASTLOS)

2.3 Bilingual Public Lectures and Recruitment Events

Example

Bibliography

- [1] A. Vieregg, K. Bechtol, and A. Romero-Wolf, "A technique for detection of pev neutrinos using a phased radio array," *Journal of Cosmology and Astroparticle Physics*, vol. 2016, p. 005, feb 2016.
- [2] J. Avva, K. Bechtol, T. Chesebro, L. Cremonesi, C. Deaconu, A. Gupta, A. Ludwig, W. Messino, C. Miki, R. Nichol, E. Oberla, M. Ransom, A. Romero-Wolf, D. Saltzberg, C. Schlupf, N. Shipp, G. Varner, A. Vieregg, and S. Wissel, "Development toward a ground-based interferometric phased array for radio detection of high energy neutrinos," *Nuclear Instruments and Methods in Physics Research Section A: Accelerators, Spectrometers, Detectors and Associated Equipment*, vol. 869, pp. 46–55, 2017.
- [3] J. C. Hanson, "Broadband rf phased array design with meep: Comparisons to array theory in two and three dimensions," *Electronics*, vol. 10, no. 4, 2021.
- [4] J. Aguilar, P. Allison, J. Beatty, H. Bernhoff, D. Besson, N. Bingefors, O. Botner, S. Buitink, K. Carter, B. Clark, A. Connolly, P. Dasgupta, S. de Kockere, K. de Vries, C. Deaconu, M. DuVernois, N. Feigl, D. García-Fernández, C. Glaser, A. Hallgren, S. Hallmann, J. Hanson, B. Hendricks, B. Hokanson-Fasig, C. Hornhuber, K. Hughes, A. Karle, J. Kelley, S. Klein, R. Krebs, R. Lahmann, M. Magnuson, T. Meures, Z. Meyers, A. Nelles, A. Novikov, E. Oberla, B. Oeyen, H. Pandya, I. Plaisier, L. Pyras, D. Ryckbosch, O. Scholten, D. Seckel, D. Smith, D. Southall, J. Torres, S. Toscano, D. V. D. Broeck, N. van Eijndhoven, A. Vieregg, C. Welling, S. Wissel, R. Young, and A. Zink, "Design and sensitivity of the radio neutrino observatory in greenland (RNO-g)," *Journal of Instrumentation*, vol. 16, p. P03025, mar 2021.
- [5] E. Arnold, C. Leuschen, F. Rodriguez-Morales, J. Li, J. Paden, R. Hale, and S. Keshmiri, "Cresis airborne radars and platforms for ice and snow sounding," *Annals of Glaciology*, vol. 61, no. 81, p. 58–67, 2020.
- [6] L. Li, J.-B. Yan, C. O'Neill, C. D. Simpson, and S. P. Gogineni, "Coplanar side-fed tightly coupled ultra-wideband array for polar ice sounding," *IEEE Transactions on Antennas and Propagation*, vol. 70, no. 6, pp. 4331–4341, 2022.
- [7] S. Hussain, S.-W. Qu, A. Sharif, H. Abubakar, X.-H. Wang, M. Imran, and Q. Abbasi, "Current sheet antenna array and 5g: Challenges, recent trends, developments, and future directions," *Sensors*, vol. 22, no. 9, 2022.
- [8] A. Fedeli, C. Montecucco, and G. L. Gragnani, "Open-Source Software for Electromagnetic Scattering Simulation: The Case of Antenna Design," *Electronics*, vol. 8, no. 12, p. 1506, 2019.
- [9] O. Yurduseven, S. Ye, T. Fromenteze, B. Wiley, and D. Smith, "3d conductive polymer printed metasurface antenna for fresnel focusing," *Designs*, vol. 3, no. 46, 2019.
- [10] F. Pizarro, R. Salazar, E. Rajo-Iglesias, M. Rodríguez, S. Fingerhuth, and G. Hermosilla, "Parametric study of 3d additive printing parameters using conductive filaments on microwave topologies," *IEEE Access*, vol. 7, pp. 106814–106823, 2019.
- [11] J. Hanson, "Broadband rf phased array design with meep." MeepCon 2022, 2022.
- [12] A. F. Oskooi, D. Roundy, M. Ibanescu, P. Bermel, J. Joannopoulos, and S. G. Johnson, "Meep: A flexible free-software package for electromagnetic simulations by the FDTD method," *Computer Physics Communications*, vol. 181, no. 3, pp. 687–702, 2010.
- [13] P. Allison and et al, "Low-threshold ultrahigh-energy neutrino search with the askaryan radio array," *Phys. Rev. D*, vol. 105, p. 122006, Jun 2022.
- [14] Anker, A, et al, "Probing the angular and polarization reconstruction of the ARIANNA detector at the South Pole," *Journal of Instrumentation*, vol. 15, no. 09, pp. P09039–P09039, 2020.
- [15] M. Estrada, "Creating pathways of kindness and inclusion in stem education." Inclusivity in Introductory STEM Courses, 2022.
- [16] C. Singh, "Promoting equity in science learning." Inclusivity in Introductory STEM Courses, 2022.

- [17] C. Freeman, A. Kittredge, H. Wilson, and B. Pajak, "The duolingo method for app-based teaching and learning," tech. rep., Duolingo Research Report, 2023.
- [18] D. Shin and J. Shim, "A systematic review on data mining for mathematics and science education," *International Journal of Science and Mathematics Education*, pp. 1–21, 2020.
- [19] C. Cooper and P. Pearson, "A genetically optimized predictive system for success in general chemistry using a diagnostic algebra test," *Journal of Science Education and Technology*, vol. 21, no. 1, 2011.
- [20] J. Grossman, Z. Lin, H. Sheng, J. Wei, J. Williams, and S. Goel, "Mathbot: Transforming online resources for learning math into conversational interactions," *Association for the Advancement of Artificial Intelligence (www.aaai.org)*, 2019.
- [21] H. Lee and "et al", "Automated text scoring and real-time adjustable feedback: Supporting revision of scientific arguments involving uncertainty," *Science Education Journal*, vol. 103, no. 3, 2019.
- [22] J. Ghimire, F. D. Diba, J.-H. Kim, and D.-Y. Choi, "Vivaldi Antenna Arrays Feed by Frequency-Independent Phase Shifter for High Directivity and Gain Used in Microwave Sensing and Communication Applications," *Sensors (Basel, Switzerland)*, vol. 21, no. 18, p. 6091, 2021.
- [23] F. Cui, G. Dong, Y. Chen, C. Wang, D. Teng, and R. Wang, "Numerical modeling and data signal analysis of GPR array based on dual-field domain-decomposition time-domain finite element method," *Journal of Applied Geophysics*, vol. 208, p. 104876, 2023.
- [24] R. Mailloux, *The Phased Array Handbook*, 3rd ed. Boston: Artech House, 2017.
- [25] "Xfdtd 3d electromagnetic simulation software." <https://www.remcom.com>. Accessed: 2023-05-23.
- [26] "Ansys hfss." <https://www.ansys.com>. Accessed: 2023-05-23.
- [27] O. Yurduseven, P. Flowers, S. Ye, D. L. Marks, J. N. Gollub, T. Fromenteze, B. J. Wiley, and D. R. Smith, "Computational microwave imaging using 3D printed conductive polymer frequency-diverse metasurface antennas," *IET Microwaves, Antennas & Propagation*, vol. 11, no. 14, pp. 1962–1969, 2017.
- [28] K. Yee, "Numerical solution of initial boundary value problems involving maxwell's equations in isotropic media," *IEEE Transactions on Antennas and Propagation*, vol. 14, no. 3, pp. 302–307, 1966.
- [29] A. Hammond, "High-performance topology optimization for photonics inverse design." MeepCon 2022, 2022.
- [30] The IceCube Collaboration, "Evidence for High-Energy Extraterrestrial Neutrinos at the IceCube Detector," *Science*, vol. 342, no. 6161, pp. 1242856–1242856, 2013.
- [31] M. Ackermann et al, "Astrophysics Uniquely Enabled by Observations of High-Energy Cosmic Neutrinos," 2019.
- [32] M. Ackermann et al, "Fundamental Physics with High-Energy Cosmic Neutrinos," 2019.
- [33] M. Ahlers, L. Anchordoqui, M. Gonzalez-Garcia, F. Halzen, and S. Sarkar, "GZK neutrinos after the Fermi-LAT diffuse photon flux measurement," *Astroparticle Physics*, vol. 34, no. 2, pp. 106–115, 2010.
- [34] K. Kotera, D. Allard, and A. Olinto, "Cosmogenic neutrinos: parameter space and detectability from PeV to ZeV," *Journal of Cosmology and Astroparticle Physics*, vol. 2010, no. 10, p. 013, 2010.
- [35] The IceCube Collaboration, "Differential limit on the extremely-high-energy cosmic neutrino flux in the presence of astrophysical background from nine years of IceCube data," *Physical Review D*, vol. 98, no. 6, p. 062003, 2018.
- [36] The ARIANNA Collaboration, "A search for cosmogenic neutrinos with the ARIANNA test bed using 4.5 years of data," *Journal of Cosmology and Astroparticle Physics*, vol. 2020, no. 03, pp. 053–053, 2020.
- [37] P. Allison, S. Archambault, J. J. Beatty, M. Beheler-Amass, D. Z. Besson, M. Beydler, C. C. Chen, C. H. Chen, P. Chen, B. A. Clark, W. Clay, A. Connolly, L. Cremonesi, J. Davies, S. d. Kockere, K. D. d. Vries, C. Deaconu, M. A. DuVernois, E. Friedman, R. Gaivor, J. Hanson, K. Hanson, K. D. Hoffman, B. Hokanson-Fasig, E. Hong, S. Y. Hsu, L. Hu, J. J. Huang, M. H. Huang, K. Hughes, A. Ishihara, A. Karle, J. L. Kelley, R. Khandelwal, K. C. Kim, M. C. Kim, I. Kravchenko, K. Kurusu, H. Landsman, U. A. Latif, A. Laundrie, C. J. Li, T. C. Liu, M. Y. Lu, B. Madison, K. Mase, T. Meures, J. Nam, R. J. Nichol, G. Nir, A. Novikov, A. Nozdrina, E. Oberla, A. O'Murchadha, J. Osborn, Y. Pan, C. Pfendner, J. Roth, P. Sandstrom, D. Seckel, Y. S. Shiao, A. Shultz, D. Smith, J. Torres, J. Touart, N. v. Eijndhoven, G. S. Varner, A. G. Vieregg, M. Z. Wang, S. H. Wang, S. A. Wissel, S. Yoshida, R. Young, and A. Collaboration, "Constraints on the diffuse flux of ultrahigh energy neutrinos from four years of Askaryan Radio Array data in two stations," *Physical Review D*, vol. 102, no. 4, p. 043021, 2020.
- [38] J. C. Hanson, S. W. Barwick, E. C. Berg, D. Z. Besson, T. J. Duffin, S. R. Klein, S. A. Kleinfelder, C. Reed, M. Roumi, T. Stezelberger, J. Tatar, J. A. Walker, and L. Zou, "Radar absorption, basal reflection, thickness and polarization measurements from the Ross Ice Shelf, Antarctica," *Journal of Glaciology*, vol. 61, no. 227, pp. 438–446, 2015.

- [39] J. Avva, J. Kovac, C. Miki, D. Saltzberg, and A. Vieregg, "An in situ measurement of the radio-frequency attenuation in ice at Summit Station, Greenland," *Journal of Glaciology*, 2014.
- [40] P. Allison, J. Auffenberg, R. Bard, J. Beatty, D. Besson, S. Böser, C. Chen, P. Chen, A. Connolly, and J. Davies, "Design and initial performance of the Askaryan Radio Array prototype EeV neutrino detector at the South Pole," *Astroparticle Physics*, vol. 35, no. 7, pp. 457–477, 2012.
- [41] G. Askaryan, "Cherenkov Radiation and Transition Radiation from Electromagnetic Waves," *Soviet Physics JETP*, vol. 15, no. 5, 1962.
- [42] E. Zas, F. Halzen, and T. Stanev, "Electromagnetic pulses from high-energy showers: Implications for neutrino detection," *Physical Review D*, vol. 45, no. 1, p. 362, 1992.
- [43] I. Kravchenko et al, "Updated results from the RICE experiment and future prospects for ultra-high energy neutrino detection at the south pole," *Physical Review D*, vol. 85, no. 6, p. 062004, 2012.
- [44] The ANITA Collaboration, "Constraints on the ultrahigh-energy cosmic neutrino flux from the fourth flight of ANITA," *Physical Review D*, vol. 99, no. 12, p. 122001, 2019.
- [45] D. Saltzberg, P. Gorham, D. Walz, C. Field, R. Iverson, A. Odian, G. Resch, P. Schoessow, and D. Williams, "Observation of the Askaryan effect: coherent microwave Cherenkov emission from charge asymmetry in high-energy particle cascades.," *Physical review letters*, vol. 86, no. 13, pp. 2802–5, 2001.
- [46] P. Miocinovic, R. Field, P. Gorham, E. Guilliam, R. Milincic, D. Saltzberg, D. Walz, and D. Williams, "Time-domain measurement of broadband coherent Cherenkov radiation," *Physical Review D*, vol. 74, no. 4, p. 043002, 2006.
- [47] P. W. Gorham, S. W. Barwick, J. J. Beatty, D. Z. Besson, W. R. Binns, C. Chen, P. Chen, J. M. Clem, A. Connolly, P. F. Dowkontt, M. A. DuVernois, R. C. Field, D. Goldstein, A. Goodhue, C. Hast, C. L. Hebert, S. Hoover, M. H. Israel, J. Kowalski, J. G. Learned, K. M. Liewer, J. T. Link, E. Lusczek, S. Matsuno, B. Mercurio, C. Miki, P. Miocinović, J. Nam, C. J. Naudet, J. Ng, R. Nichol, K. Palladino, K. Reil, A. Romero-Wolf, M. Rosen, L. Ruckman, D. Saltzberg, D. Seckel, G. S. Varner, D. Walz, and F. Wu, "Observations of the askaryan effect in ice," *Phys. Rev. Lett.*, vol. 99, p. 171101, Oct 2007.
- [48] J. C. Hanson and R. Hartig, "Complex analysis of askaryan radiation: A fully analytic model in the time domain," *Phys. Rev. D*, vol. 105, p. 123019, Jun 2022.
- [49] K. Dookayka, *Characterizing the Search for Ultra-High Energy Neutrinos with the ARIANNA Detector* DISSERTATION. PhD thesis, University of California, Irvine, 2011.
- [50] The ARA Collaboration, "First constraints on the ultra-high energy neutrino flux from a prototype station of the askaryan radio array," *Astroparticle Physics*, vol. 70, pp. 62–80, 2015.
- [51] C. Glaser, D. García-Fernández, A. Nelles, J. Alvarez-Muñiz, S. W. Barwick, D. Z. Besson, B. A. Clark, A. Connolly, C. Deaconu, K. D. d. Vries, J. C. Hanson, B. Hokanson-Fasig, R. Lahmann, U. Latif, S. A. Kleinfelder, C. Persichilli, Y. Pan, C. Pfendner, I. Plaisier, D. Seckel, J. Torres, S. Toscano, N. v. Eijndhoven, A. Vieregg, C. Welling, T. Winchen, and S. A. Wissel, "NuRadioMC: simulating the radio emission of neutrinos from interaction to detector," *The European Physical Journal C*, vol. 80, no. 2, p. 77, 2020.
- [52] C. Glaser, A. Nelles, I. Plaisier, C. Welling, S. W. Barwick, D. García-Fernández, G. Gaswint, R. Lahmann, and C. Persichilli, "NuRadioReco: a reconstruction framework for radio neutrino detectors," *The European Physical Journal C*, vol. 79, no. 6, p. 464, 2019.
- [53] C. Welling, P. Frank, T. A. Enßlin, and A. Nelles, "Reconstructing non-repeating radio pulses with Information Field Theory," *arXiv*, 2021.
- [54] S. Barwick, E. Berg, D. Besson, T. Duffin, J. Hanson, S. Klein, S. Kleinfelder, M. Piasecki, K. Ratzlaff, C. Reed, M. Roumi, T. Stezelberger, J. Tatar, J. Walker, R. Young, and L. Zou, "Time-domain response of the ARIANNA detector," *Astroparticle Physics*, vol. 62, pp. 139–151, 2015.
- [55] S. W. Barwick, E. C. Berg, D. Z. Besson, G. Gaswint, C. Glaser, A. Hallgren, J. C. Hanson, S. R. Klein, S. Kleinfelder, L. Köpke, I. Kravchenko, R. Lahmann, U. Latif, J. Nam, A. Nelles, C. Persichilli, P. Sandstrom, J. Tatar, and E. Unger, "Observation of classically 'forbidden' electromagnetic wave propagation and implications for neutrino detection.," *Journal of Cosmology and Astroparticle Physics*, vol. 2018, no. 07, pp. 055–055, 2018.
- [56] The ARA Collaboration, "Measurement of the real dielectric permittivity ϵ_r of glacial ice," *Astroparticle Physics*, vol. 108, pp. 63–73, 2019.
- [57] S. Barwick, E. Berg, D. Besson, G. Binder, W. Binns, D. Boersma, R. Bose, D. Braun, J. Buckley, V. Bugaev, S. Buitink, K. Dookayka, P. Dowkontt, T. Duffin, S. Euler, L. Gerhardt, L. Gustafsson, A. Hallgren, J. Hanson, M. Israel, J. Kiryluk, S. Klein, S. Kleinfelder, H. Niederhausen, M. Olevitch, C. Persichilli, K. Ratzlaff, B. Rauch, C. Reed, M. Roumi, A. Samanta, G. Simburger, T. Stezelberger, J. Tatar, U. Uggerhoj, J. Walker, G. Yodh, and R. Young, "A first search for cosmogenic neutrinos with the ARIANNA Hexagonal Radio Array," *Astroparticle Physics*, vol. 70, pp. 12–26, 2015.

- [58] S. Barwick, D. Besson, A. Burgman, E. Chiem, A. Hallgren, J. Hanson, S. Klein, S. Kleinfelder, A. Nelles, C. Persichilli, S. Phillips, T. Prakash, C. Reed, S. Shively, J. Tatar, E. Unger, J. Walker, and G. Yodh, "Radio detection of air showers with the arianna experiment on the ross ice shelf," *Astroparticle Physics*, 2016.
- [59] J A Aguilar et al, "Design and Sensitivity of the Radio Neutrino Observatory in Greenland (RNO-G)," *arXiv*, 2020.
- [60] S. Barwick, E. Berg, D. Besson, G. Gaswint, C. Glaser, A. Hallgren, J. Hanson, S. Klein, S. Kleinfelder, L. Köpke, I. Kravchenko, R. Lahmann, U. Latif, J. Nam, A. Nelles, C. Persichilli, P. Sandstrom, J. Tatar, and E. Unger, "Observation of classically 'forbidden' electromagnetic wave propagation and implications for neutrino detection.," *Journal of Cosmology and Astroparticle Physics*, vol. 2018, no. 07, p. 055, 2018.
- [61] C. Deaconu, A. G. Vieregg, S. A. Wissel, J. Bowen, S. Chipman, A. Gupta, C. Miki, R. J. Nichol, and D. Saltzberg, "Measurements and modeling of near-surface radio propagation in glacial ice and implications for neutrino experiments," *Phys. Rev. D*, vol. 98, p. 043010, Aug 2018.
- [62] The IceCube Gen2 Collaboration, "Icecube-gen2: the window to the extreme universe," *Journal of Physics G: Nuclear and Particle Physics*, vol. 48, p. 060501, apr 2021.
- [63] S. Barwick, E. Berg, D. Besson, T. Duffin, J. Hanson, S. Klein, S. Kleinfelder, K. Ratzlaff, C. Reed, M. Roumi, T. Stezelberger, J. Tatar, J. Walker, R. Young, and L. Zou, "Design and Performance of the ARIANNA HRA-3 Neutrino Detector Systems," *IEEE Transactions on Nuclear Science*, vol. 62, no. 5, pp. 2202–2215, 2015.
- [64] S. W. Barwick *et al.*, "A First Search for Cosmogenic Neutrinos with the ARIANNA Hexagonal Radio Array," *Astropart. Phys.*, vol. 70, pp. 12–26, 2015.
- [65] J. Hanson, "Broadband RF Phased Array Design for UHE neutrino detection," *Proceedings of 37th International Cosmic Ray Conference — PoS(ICRC2021)*, p. 1217, 2021.
- [66] S. Barwick, D. Besson, P. Gorham, and D. Saltzberg, "South polar in situ radio-frequency ice attenuation," *Journal of Glaciology*, vol. 51, no. 173, p. 231–238, 2005.
- [67] M. Stockham, J. Macy, and D. Besson, "Radio frequency ice dielectric permittivity measurements using CReSIS data," *Radio Science*, vol. 51, no. 3, pp. 194–212, 2016.